

# Fabrication and surface treatment of electron-beam evaporated niobium for low-loss coplanar waveguide resonators

Cite as: Appl. Phys. Lett. **119**, 132601 (2021); <https://doi.org/10.1063/5.0066441>

Submitted: 10 August 2021 • Accepted: 09 September 2021 • Published Online: 27 September 2021

 D. Kowsari,  K. Zheng,  J. T. Monroe, et al.



View Online



Export Citation



CrossMark

## ARTICLES YOU MAY BE INTERESTED IN

### Materials loss measurements using superconducting microwave resonators

Review of Scientific Instruments **91**, 091101 (2020); <https://doi.org/10.1063/5.0017378>

### Tailoring broadband Kerr soliton microcombs via post-fabrication tuning of the geometric dispersion

Applied Physics Letters **119**, 121103 (2021); <https://doi.org/10.1063/5.0061238>

### A quantum engineer's guide to superconducting qubits

Applied Physics Reviews **6**, 021318 (2019); <https://doi.org/10.1063/1.5089550>

Lock-in Amplifiers  
up to 600 MHz



Zurich  
Instruments



# Fabrication and surface treatment of electron-beam evaporated niobium for low-loss coplanar waveguide resonators

Cite as: Appl. Phys. Lett. **119**, 132601 (2021); doi: [10.1063/5.0066441](https://doi.org/10.1063/5.0066441)

Submitted: 10 August 2021 · Accepted: 9 September 2021 ·

Published Online: 27 September 2021



[View Online](#)



[Export Citation](#)



[CrossMark](#)

D. Kowsari,<sup>1,a)</sup>  K. Zheng,<sup>1</sup>  J. T. Monroe,<sup>1</sup>  N. J. Thobaben,<sup>2</sup>  X. Du,<sup>1</sup>  P. M. Harrington,<sup>1,3</sup>  E. A. Henriksen,<sup>1,4</sup>  D. S. Wisbey,<sup>2,a)</sup>  and K. W. Murch<sup>1,a)</sup> 

## AFFILIATIONS

<sup>1</sup>Department of Physics, Washington University, Saint Louis, Missouri 63130, USA

<sup>2</sup>Department of Physics, Saint Louis University, Saint Louis, Missouri 63103, USA

<sup>3</sup>Research Laboratory of Electronics, Massachusetts Institute of Technology, Cambridge, Massachusetts 02139, USA

<sup>4</sup>Institute for Materials Science and Engineering, Washington University, Saint Louis, Missouri 63130, USA

<sup>a)</sup>Authors to whom correspondence should be addressed: [dariakowsari@wustl.edu](mailto:dariakowsari@wustl.edu); [david.wisbey@slu.edu](mailto:david.wisbey@slu.edu); and [murch@physics.wustl.edu](mailto:murch@physics.wustl.edu)

## ABSTRACT

We characterize low-loss electron-beam evaporated niobium thin films deposited under ultra-high vacuum conditions. Slow deposition yields films with a high superconducting transition temperature ( $9.20 \pm 0.06$  K) as well as a residual resistivity ratio of 4.8. We fabricate the films into coplanar waveguide resonators to extract the intrinsic loss due to the presence of two-level-system fluctuators using microwave measurements. For a coplanar waveguide resonator gap of  $2 \mu\text{m}$ , the films exhibit filling-factor-adjusted two-level-system loss tangents as low as  $1.5 \times 10^{-7}$  with single-photon regime internal quality factors in excess of one million after removing native surface oxides of the niobium.

Published under an exclusive license by AIP Publishing. <https://doi.org/10.1063/5.0066441>

Recent achievements in quantum computing have shown that superconducting circuits are one of the most promising platforms to realize the long-sought challenge of building a fault-tolerant quantum computer.<sup>1–3</sup> The performance of such devices is, however, limited by decoherence sources such as quasiparticles,<sup>4–6</sup> magnetic vortices,<sup>7</sup> and radiation effects.<sup>8</sup> Recent advances in fabrication techniques and microwave engineering have significantly reduced the impacts of the above-mentioned defects,<sup>9–11</sup> thereby leaving two-level-system (TLS) fluctuators as the most prominent source of loss in superconducting circuits.<sup>12–14</sup> It has been shown that TLS defects are mainly located at metal–air (MA), substrate–air (SA), and metal–substrate (MS) interfaces.<sup>15–19</sup> The contribution of losses from these interfaces can be minimized by implementing careful surface treatments, thus enhancing the coherence of the devices.<sup>20,21</sup>

Owing to its high superconducting transition temperature, critical field, and low microwave loss,<sup>22</sup> niobium (Nb) has become one of the common materials used in the fabrication of superconducting circuits.<sup>23,24</sup> Nevertheless, the known stoichiometric range of its native oxides results in a complex loss-inducing MA interface.<sup>25,26</sup> Lately, it has been shown that removing the oxides on the MA interface of Nb films

can result in highly coherent devices.<sup>27,28</sup> Additionally, conventional niobium deposition techniques, such as DC magnetron sputtering, can result in a damaged MS interface due to the presence of high energy argon ions<sup>29</sup> and point defects stemming from trapped argon atoms.<sup>30</sup>

In order to prevent these sources of decoherence, here we investigate a refined deposition method<sup>31</sup> of Nb utilizing an ultra-high vacuum (UHV) electron-beam evaporator. We fabricate the Nb thin films into coplanar waveguide (CPW) resonators, which are well-known for their ease of fabrication as well as their sensitivity to the true intrinsic TLS defect density of the materials.<sup>15,32</sup> We observe that surface treatment results in lower TLS densities compared to prior studies using the same CPW geometry optimized for sensitivity to TLS defects.<sup>8,15,33,34</sup> This study further establishes Nb, with appropriate surface treatment, as an ideal material for the fabrication of highly coherent superconducting qubit processors.

Samples are fabricated on a 2-in., (100)-oriented, high resistivity ( $>8 \text{ k}\Omega \cdot \text{cm}$ ), single-side polished intrinsic silicon substrate cleaned in a Piranha solution (3:1 mixture of sulfuric acid and hydrogen peroxide) at  $120^\circ\text{C}$  for 10 min followed by a 5-min etch in a buffered-oxide-etch (BOE) solution to remove organic contaminants as well as

the native silicon surface oxide.<sup>20,35</sup> The BOE solution is a 6:1 mixture of ammonium fluoride ( $\text{NH}_4\text{F}$ ) and hydrofluoric acid (HF). The substrate is then pumped down in a UHV electron-beam evaporator (AJA ATC-ORION-8E) with a base pressure lower than 5 nTorr.

After loading the wafer, a 200 nm layer of 99.95% purity Nb is evaporated onto the substrate at a rate of 1.2 nm/min, which is commensurate to the previous study.<sup>31</sup> Note that the substrate is inevitably heated during this process due to the high melting point of Nb. Since pure Nb quickly adsorbs impurities,<sup>22</sup> especially when heated, we let the sample remain under UHV conditions to cooldown for 1–2 h prior to proceeding to the next steps.

We spin and softbake the Nb samples with a high resolution photoresist (MicroChem S1805) and pattern the coated wafer with a Heidelberg DWL 66+ photolithography system. The pattern consists of eight hanger-style, quarter-wavelength CPW resonators with a gap (width) of 2  $\mu\text{m}$  (3  $\mu\text{m}$ ). Devices are simulated to have frequencies ranging from 5.2 to 7 GHz with coupling quality factors  $\sim 6 \times 10^5$  (simulated using SONNET microwave software). We develop the exposed resist by using a metal-ion-free solution (MicroChem MF-319). A reactive ion etch system (Oxford Plasmalab 100) is then used to etch the samples using a fluorine chemistry ( $\text{SF}_6$ ). To assist the removal of the residual resist, the samples are first ashed for 30 s using oxygen plasma (Plasma Etch PE 50, 100 W, 15 cc/min) and then soaked in N-Methyl-2-pyrrolidone (NMP) heated to 70 °C for 8 h. At last, samples are coated with the photoresist (S1805) to enhance their preservation over time<sup>27</sup> and protect against damage caused by dicing.

Figure 1 illustrates the surface topography of the Nb films fabricated into CPWs [Fig. 1(a)] using the above-mentioned techniques. The scanning electron microscopy (SEM) image shows the elongated Nb grains formed on the surface [Fig. 1(b)]. The dark-field scanning transmission electron microscopy (STEM) cross-sectional image of the etched films shows that our etching process is anisotropic [Fig. 1(c)]. In this study, the etching has been engineered to result in trenches shallower than 500 nm for all the fabricated devices to maintain the effective substrate dielectric constant in the devices, and thereby to avoid deviations from the desired resonance frequencies.<sup>33</sup> The STEM image shows grain sizes greater than 20 nm [Fig. 1(d)], exceeding previous values reported using the same deposition technique.<sup>31</sup> Correlation between the grain sizes and materials loss has been recently studied,<sup>36</sup> substantiating the advantage of larger grain sizes by treating the grain boundaries as Josephson weak-links.<sup>37</sup> Finally, the films resulted in a superconducting transition temperature  $T_c = 9.20 \pm 0.06$  K and a residual resistivity ratio (RRR) of 4.8 [Fig. 1(e)], exhibiting the high quality of the evaporated Nb in accord with recent results with sputtered Nb.<sup>36</sup> Note that the films deposited at higher pressures ( $>6$  nTorr) resulted in a significantly lower transition temperature  $T_c \simeq 7.85$  K as well as a RRR of only 1.8, which can be attributed to the fact that having a low deposition rate makes the quality of the films extremely sensitive to the deposition environment. Therefore, having a UHV deposition environment is a crucial condition for achieving high quality films using this technique.

Transmission electron microscopy (TEM) images show a clear band of about 5 nm of oxide on top of the Nb, which is reduced to  $\sim 1.7$  nm after removing the surface oxides in a BOE solution for 20 min [Figs. 2(a) and 2(b)]. Note that it takes about 20 min to transfer the sample to the characterization instruments, during which the oxide grows back following the Cabrera–Mott theory.<sup>28</sup> To identify the elements present in the

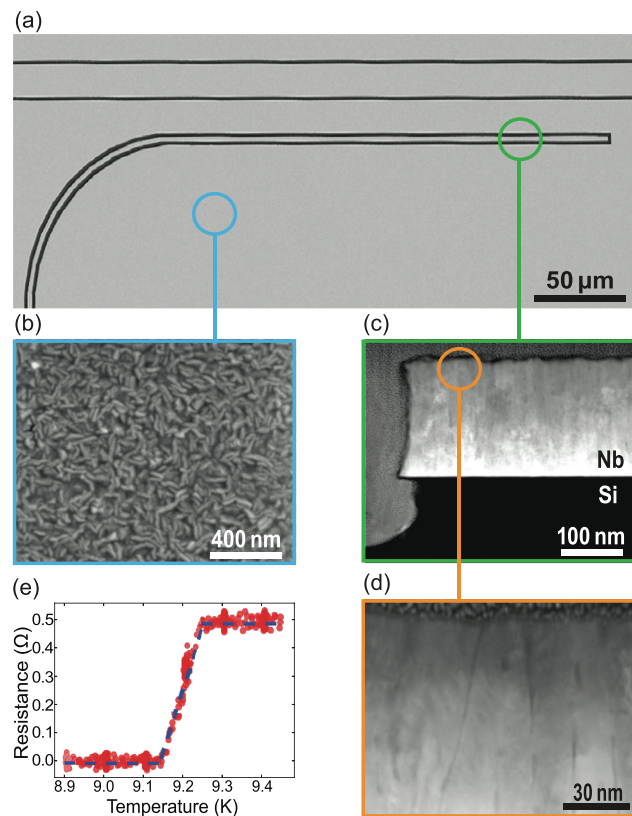
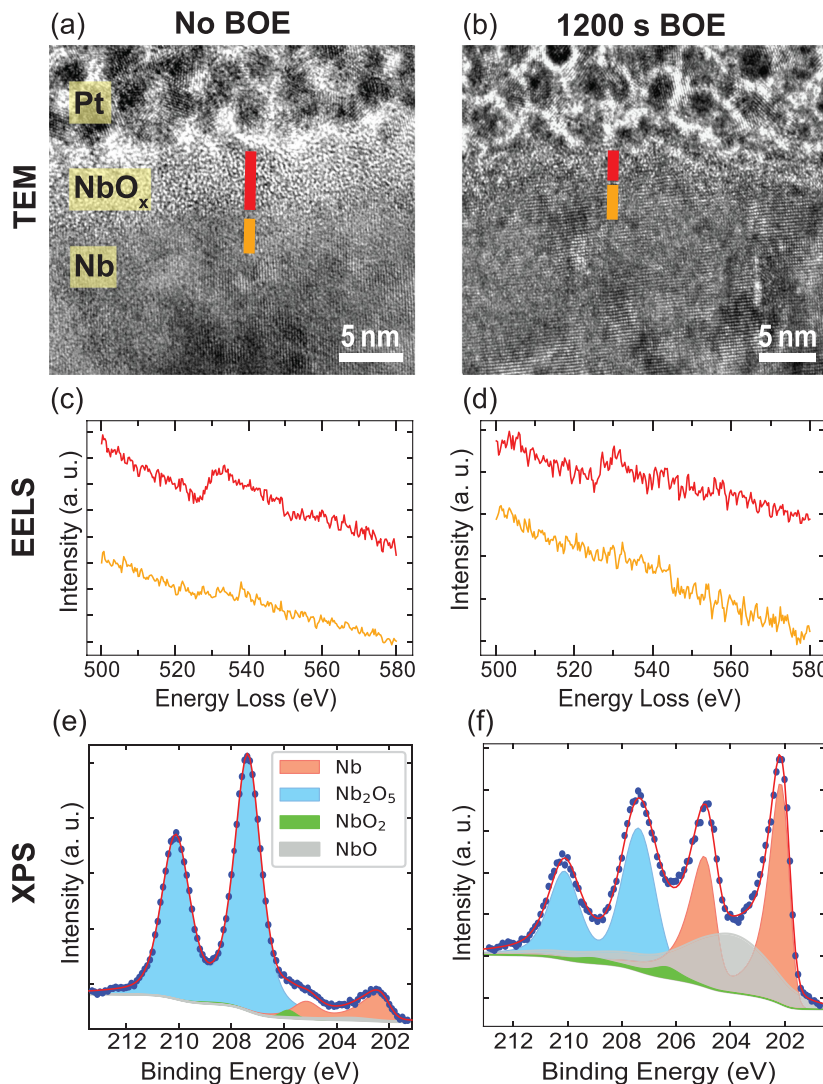


FIG. 1. Surface topography of the fabricated CPWs. (a) SEM image shows the fabricated resonator coupled to the feedline with a CPW gap of 2  $\mu\text{m}$ . (b) Detailed SEM image displays the compact elongated niobium grains formed on the surface. (c) A dark-field STEM cross-sectional image illustrates the anisotropic etch. (d) A STEM cross-sectional image depicts grain sizes exceeding 20 nm. (e) The four-probe resistance measurement shows a superconducting transition temperature  $T_c = 9.20 \pm 0.06$  K. The uncertainty in the transition temperature is taken as the full temperature range of the transition. The RRR is calculated by dividing the surface resistance at 310 K to that right before the transition at 9.258 K as  $2.33\Omega/0.49\Omega \simeq 4.8$  exhibiting high quality of the films.

films, we perform electron-energy loss spectroscopy (EELS) measurements. Averaged EELS spectra are displayed in Figs. 2(c) and 2(d) along the red (orange) lines for the oxide (metal) regions of the TEM images in Figs. 2(a) and 2(b). The regions indicated by red lines exhibit a clear peak located at  $\sim 535$  eV, which corresponds to the presence of oxygen. Below this  $\text{NbO}_x$  band, there is no sign of this peak. Furthermore, EELS data revealed a clear reduction in the average oxygen content from  $\sim 50\%$  in the oxide band to less than 5% while scanning inside the metallic Nb film indicating the absence of oxygen impurities in the films.

We employ x-ray photoelectron spectroscopy (XPS) to further investigate the compounds present on the surface. Here, we utilize a PHI VersaProbe II surface analysis instrument equipped with an aluminum K-alpha x-ray source. Under the optimal neutralization settings, an overall shift of  $\sim 2.7$  eV from the nominal binding energy values is observed due to the surface charge of the Nb films. The presented data have been adjusted to account for this shift. We examine the XPS spectrum of  $\text{Nb}_{3d}$  by curve fitting the data using the Lmfit<sup>38</sup> package. The fits reveal peaks for three distinct niobium oxides



**FIG. 2.** Comparison of the metal-air interface characteristics with different cleaning schemes. TEM samples are prepared using a focused ion beam after the deposition of a platinum (Pt) protective layer on top. TEM images show (a) a clear band of NbO<sub>x</sub>  $\sim$ 5 nm thick on top of the Nb surface and (b) after cleaning the sample for 20 min with BOE, the oxide layer thickness was reduced to  $\sim$ 1.7 nm. Red and orange lines in (a) and (b) indicate regions where averaged EELS spectra are collected. [(c) and (d)] The averaged EELS spectra with orange and red traces corresponding to regions depicted in (a) and (b). The spectra in the oxide region (red) display a significant peak around 535 eV corresponding to oxygen. This peak is absent along the Nb metal (orange), showing that there is no trace of oxygen in the Nb film. (e) Nb<sub>3d</sub> XPS measurements of the Nb surface show different niobium–oxygen compounds, dominated mostly by Nb<sub>2</sub>O<sub>5</sub> oxide prior to treating the surface. (f) After surface cleaning, we observe a clear increase in the Nb peak relative to the oxides.

[Figs. 2(e) and 2(f)]. These peaks were fit using the “skewedVoigt” model for asymmetric metallic Nb peaks and the “pseudoVoigt” model for all the other peaks using a Shirley inelastic background with 3d<sub>5/2</sub> binding energies located at 202.05, 203.40, 205.84, and 207.38 eV for Nb, NbO, NbO<sub>2</sub>, and Nb<sub>2</sub>O<sub>5</sub>, respectively, for the untreated film. Among those, NbO is superconducting with a transition temperature of 1.38 K.<sup>39</sup> Nb<sub>2</sub>O<sub>5</sub> is the most thermodynamically stable state of the niobium–oxygen system with the highest binding energy ( $\sim$ 207 eV) and the lowest electrical conductivity.<sup>40</sup> Due to its various crystalline phases and physical properties, Nb<sub>2</sub>O<sub>5</sub> has been considered as one of the main sources of defects present on the surface of Nb.<sup>41</sup> NbO<sub>2</sub> also contributes to the loss due to oxygen vacancies,<sup>36</sup> which has the lowest participation in the deposited films reported here.

Prior to placement in the measurement cryostat, devices are cleaned for 7 min in an ultrasonic bath of acetone and isopropyl alcohol to remove particles on the samples and strip the protective photoresist. The transfer time to the fridge is kept under 90 min for the BOE

post-cleaned samples to minimize oxide regrowth on the devices. The samples are placed inside palladium-plated copper microwave launch packaging surrounded by Cryoperm shielding to protect the devices from infrared radiation and external magnetic fields. Mounted devices are cooled inside an adiabatic demagnetization refrigerator (ADR) with a base temperature of 50 mK.

The resonator transmission, S<sub>21</sub>, is measured using a vector network analyzer in an experimental setup described previously.<sup>16,42,43</sup> Data are collected with the ADR in the temperature regulation mode. Figure 3(a) displays the transmission near the resonance of a particular device [indicated by the arrow in Fig. 3(c)] at low power. The quality factors are extracted by employing the  $\phi$  rotation method.<sup>44</sup> Figure 3(b) displays the internal loss tangent  $\delta_{\text{int}}$  (inverse of the internal quality factor Q<sub>i</sub>) as a function of the average photon number<sup>8</sup> of the BOE-cleaned device mentioned above. Using the TLS model,<sup>32</sup> we extract the filling-factor-adjusted TLS loss tangent (F $\delta_{\text{TLS}}$ ), where F is defined as the fraction of the resonator’s total loss stored in the TLS

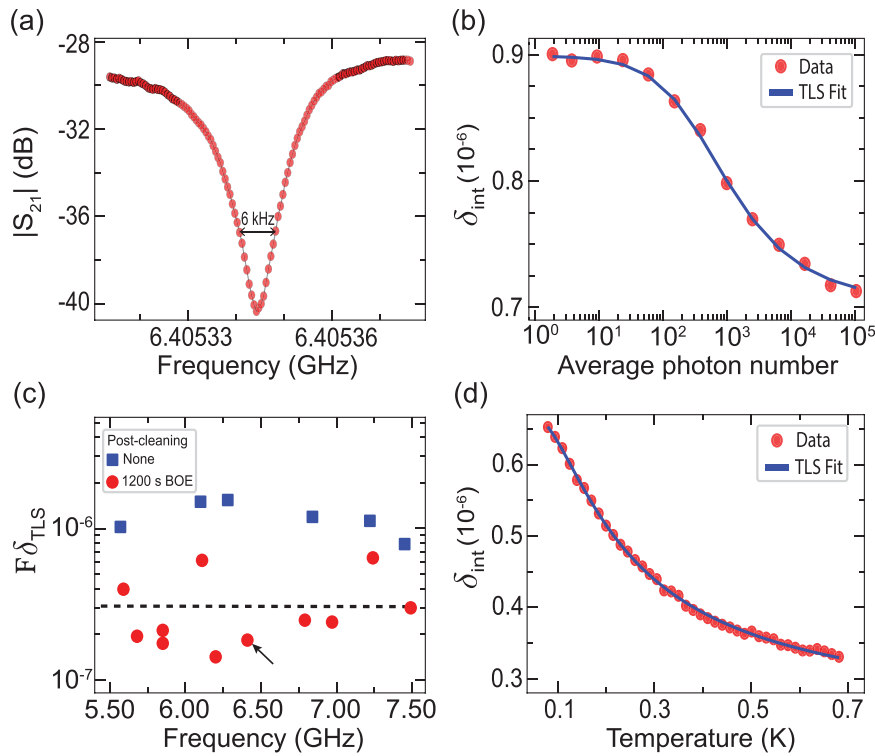


**FIG. 3.** Microwave measurements of the CPW resonators. (a) Transmission profile near the resonance at single-photon power shows a full width at half maximum of 6 kHz corresponding to an internal quality factor of  $1.06 \times 10^6$  for the device indicated by the arrow in (c). (b) The internal loss of the same device as a function of the average photon number, showing minimal dependence on power. Data points were fit using the TLS model (blue solid line), resulting in  $F\delta_{TLS} = (1.94 \pm 0.02) \times 10^{-7}$ . (c) Comparison of the extracted  $F\delta_{TLS}$  of the fabricated CPW resonators from the TLS fit of the power scans as a function of the resonance frequency across three chips for different post-cleaning treatments. Red circles indicate results for devices that were etched with a BOE solution for 1200 s before placement into a cryogenic vacuum environment for measurement. Blue squares correspond to results for samples that did not receive this pre-measurement etch treatment. The dashed line indicates the average  $F\delta_{TLS}$  value of the treated devices. (d) TLS fit of the temperature scan at high circulating power (~93 dBm), corresponding to an average photon number of  $\sim 10^5$ , resulting in  $F\delta_{TLS} = (4.39 \pm 0.02) \times 10^{-7}$ , showing a good agreement with the power scan result in (b).

material. Figure 3(c) displays  $F\delta_{TLS}$  for several devices vs resonance frequency. The  $F\delta_{TLS}$  values are an order of magnitude smaller for the case of post-cleaned devices (red circles) than the untreated devices (blue squares) resulting in values as low as 0.15 ppm. The dashed line indicates the average value of  $F\delta_{TLS}$  of the post-cleaned devices. The average value is 0.32 ppm, well below previous results using the same CPW geometry.<sup>33</sup> The average low power  $Q_i$  of the post-cleaned devices is  $1.13 \times 10^6$ . In contrast, the untreated devices (blue squares) show an average TLS loss tangent of 1.21 ppm with an average single-photon regime  $Q_i$  of  $3.35 \times 10^5$  comparable with other sputtered niobium studies.<sup>16,45</sup>

Figure 3(d) displays measurements of the internal loss of the aforementioned device vs temperature at fixed power. Based on the TLS model, the TLS-induced loss tends to saturate at high temperatures<sup>15,32</sup> as shown in Fig. 3(d). By fitting to the TLS model, we obtain a  $F\delta_{TLS}$  of 0.44 ppm in accord with the power scan.<sup>27,28,46</sup>

The above results agree with previous findings<sup>27,28,46</sup> that the MA interface is one of the main sources of TLS loss. In our study, we have employed a small CPW gap, which results in a significantly higher concentration of the electric field inside the trenches of the CPW, therefore maximizing the coupling with the TLS fluctuators at the

interfaces of the material as well as resulting in a larger filling factor value.<sup>8,34</sup> Hence, devices with larger features<sup>27</sup> would reduce this filling factor and electric field density, thereby reducing  $F\delta_{TLS}$  by nearly one order of magnitude as well as yielding higher internal quality factors.<sup>8,15</sup>

We have refined a method to deposit extremely low-loss niobium films for superconducting CPW resonators using a UHV electron-beam evaporator. With post-cleaning of the Nb surface, devices demonstrated loss tangents well-below previous limits, highlighting the role of the MA interface as one of the main sources of loss in superconducting devices. Moreover, the characterization results show a significant reduction in the surface oxide thickness, verifying the efficacy of our cleaning method. Future work may explore a practical passivation scheme to bypass the MA interface-induced losses for the fabrication of highly coherent superconducting qubit processors.

This research was supported by NSF Grant No. PHY-1752844 (CAREER), NSF Grant No. DMR-1945278 (CAREER), the John Templeton Foundation Grant No. 61835, and also acknowledge support from the institute of Materials Science and Engineering at Washington University.

## DATA AVAILABILITY

The data that support the findings of this study are available from the corresponding author upon reasonable request.

## REFERENCES

- <sup>1</sup>F. Arute, K. Arya, R. Babbush, D. Bacon, J. C. Bardin, R. Barends, R. Biswas, S. Boixo, F. G. Brandao, D. A. Buell, B. Burkett, Y. Chen, Z. Chen, B. Chiaro, R. Collins, W. Courtney, A. Dunsworth, E. Farhi, B. Foxen, A. Fowler, C. Gidney, M. Giustina, R. Graff, K. Guerin, S. Habegger, M. P. Harrigan, M. J. Hartmann, A. Ho, M. Hoffmann, T. Huang, T. S. Humble, S. V. Isakov, E. Jeffrey, Z. Jiang, D. Kafri, K. Kechedzhi, J. Kelly, P. V. Klimov, S. Knysh, A. Korotkov, F. Kostritsa, D. Landhuis, M. Lindmark, E. Lucero, D. Lyakh, S. Mandrà, J. R. McClean, M. McEwen, A. Megrant, X. Mi, K. Michielsen, M. Mohseni, J. Mutus, O. Naaman, M. Neeley, C. Neill, M. Y. Niu, E. Ostby, A. Petukhov, J. C. Platt, C. Quintana, E. G. Rieffel, P. Roushan, N. C. Rubin, D. Sank, K. J. Satzinger, V. Smelyanskiy, K. J. Sung, M. D. Trevithick, A. Vainsencher, B. Villalonga, T. White, Z. J. Yao, P. Yeh, A. Zalcman, H. Neven, and J. M. Martinis, "Quantum supremacy using a programmable superconducting processor," *Nature* **574**, 505–510 (2019).
- <sup>2</sup>P. Jurcevic, A. Javadi-Abhari, L. S. Bishop, I. Lauer, D. F. Bogorin, M. Brink, L. Capelluto, O. Günlük, T. Itoko, N. Kanazawa, A. Kandala, G. A. Keefe, K. Krsulich, W. Landers, E. P. Lewandowski, D. T. McClure, G. Nannicini, A. Narasgond, H. M. Nayfeh, E. Pritchett, M. B. Rothwell, S. Srinivasan, N. Sundaresan, C. Wang, K. X. Wei, C. J. Wood, J. B. Yau, E. J. Zhang, O. E. Dial, J. M. Chow, and J. M. Gambetta, "Demonstration of quantum volume 64 on a superconducting quantum computing system," *Quantum Sci. Technol.* **6**, 025020 (2021).
- <sup>3</sup>Y. Wu, W.-S. Bao, S. Cao, F. Chen, M.-C. Chen, X. Chen, T.-H. Chung, H. Deng, Y. Du, D. Fan, M. Gong, C. Guo, C. Guo, S. Guo, L. Han, L. Hong, H.-L. Huang, Y.-H. Huo, L. Li, N. Li, S. Li, Y. Li, F. Liang, C. Lin, J. Lin, H. Qian, D. Qiao, H. Rong, H. Su, L. Sun, L. Wang, S. Wang, D. Wu, Y. Xu, K. Yan, W. Yang, Y. Yang, Y. Ye, J. Yin, C. Ying, J. Yu, C. Zha, C. Zhang, H. Zhang, K. Zhang, Y. Zhang, H. Zhao, Y. Zhao, L. Zhou, Q. Zhu, C.-Y. Lu, C.-Z. Peng, X. Zhu, and J.-W. Pan, "Strong quantum computational advantage using a superconducting quantum processor," *arXiv:2106.14734* (2021).
- <sup>4</sup>P. J. De Visser, D. J. Goldie, P. Diener, S. Withington, J. J. Baselmans, and T. M. Klapwijk, "Evidence of a nonequilibrium distribution of quasiparticles in the microwave response of a superconducting aluminum resonator," *Phys. Rev. Lett.* **112**, 047004 (2014).
- <sup>5</sup>R. Barends, J. Wenner, M. Lenander, Y. Chen, R. C. Bialczak, J. Kelly, E. Lucero, P. O'Malley, M. Mariantoni, D. Sank, H. Wang, T. C. White, Y. Yin, J. Zhao, A. N. Cleland, J. M. Martinis, and J. J. Baselmans, "Minimizing quasiparticle generation from stray infrared light in superconducting quantum circuits," *Appl. Phys. Lett.* **99**, 113507 (2011).
- <sup>6</sup>A. D. Córcoles, J. M. Chow, J. M. Gambetta, C. Rigetti, J. R. Rozen, G. A. Keefe, M. B. Rothwell, M. B. Ketchen, and M. Steffen, "Protecting superconducting qubits from radiation," *Appl. Phys. Lett.* **99**, 181906 (2011).
- <sup>7</sup>C. Song, T. W. Heitmann, M. P. Defeo, K. Yu, R. McDermott, M. Neeley, J. M. Martinis, and B. L. Plourde, "Microwave response of vortices in superconducting thin films of Re and Al," *Phys. Rev. B* **79**, 174512 (2009).
- <sup>8</sup>J. M. Sage, V. Bolkhovsky, W. D. Oliver, B. Turek, and P. B. Welander, "Study of loss in superconducting coplanar waveguide resonators," *J. Appl. Phys.* **109**, 063915 (2011).
- <sup>9</sup>J. M. Kreikebaum, A. Dove, W. Livingston, E. Kim, and I. Siddiqi, "Optimization of infrared and magnetic shielding of superconducting TiN and Al coplanar microwave resonators," *Supercond. Sci. Technol.* **29**, 104002 (2016).
- <sup>10</sup>M. Sandberg, M. R. Vissers, T. A. Ohki, J. Gao, J. Aumentado, M. Weides, and D. P. Pappas, "Radiation-suppressed superconducting quantum bit in a planar geometry," *Appl. Phys. Lett.* **102**, 072601 (2013).
- <sup>11</sup>B. Chiaro, A. Megrant, A. Dunsworth, Z. Chen, R. Barends, B. Campbell, Y. Chen, A. Fowler, I. C. Hoi, E. Jeffrey, J. Kelly, J. Mutus, C. Neill, P. J. O'Malley, C. Quintana, P. Roushan, D. Sank, A. Vainsencher, J. Wenner, T. C. White, and J. M. Martinis, "Dielectric surface loss in superconducting resonators with flux-trapping holes," *Supercond. Sci. Technol.* **29**, 104006 (2016).
- <sup>12</sup>J. Lisenfeld, A. Bilmes, A. Megrant, R. Barends, J. Kelly, P. Klimov, G. Weiss, J. M. Martinis, and A. V. Ustinov, "Electric field spectroscopy of material defects in transmon qubits," *npj Quantum Inf.* **5**, 105 (2019).
- <sup>13</sup>S. E. de Graaf, L. Faoro, L. B. Ioffe, S. Mahashabde, J. J. Burnett, T. Lindström, S. E. Kubatkin, A. V. Danilov, and A. Y. Tzalenchuk, "Two-level systems in superconducting quantum devices due to trapped quasiparticles," *Sci. Adv.* **6**, abc5055 (2020).
- <sup>14</sup>D. Niegce, J. J. Burnett, M. G. Latorre, and J. Bylander, "Geometric scaling of two-level-system loss in superconducting resonators," *Supercond. Sci. Technol.* **33**, 025013 (2020).
- <sup>15</sup>J. Gao, M. Daal, A. Vayonakis, S. Kumar, J. Zmuidzinas, B. Sadoulet, B. A. Mazin, P. K. Day, and H. G. Leduc, "Experimental evidence for a surface distribution of two-level systems in superconducting lithographed microwave resonators," *Appl. Phys. Lett.* **92**, 152505 (2008).
- <sup>16</sup>D. S. Wisbey, J. Gao, M. R. Vissers, F. C. Da Silva, J. S. Kline, L. Vale, and D. P. Pappas, "Effect of metal/substrate interfaces on radio-frequency loss in superconducting coplanar waveguides," *J. Appl. Phys.* **108**, 093918 (2010).
- <sup>17</sup>A. Bilmes, A. Megrant, P. Klimov, G. Weiss, J. M. Martinis, A. V. Ustinov, and J. Lisenfeld, "Resolving the positions of defects in superconducting quantum bits," *Sci. Rep.* **10**, 3090 (2020).
- <sup>18</sup>L. Grünhaupt, U. Von Lüpke, D. Gusekova, S. T. Skacel, N. Maleeva, S. Schliör, A. Bilmes, H. Rotzinger, A. V. Ustinov, M. Weides, and I. M. Pop, "An argon ion beam milling process for native AlO<sub>x</sub> layers enabling coherent superconducting contacts," *Appl. Phys. Lett.* **111**, 072601 (2017).
- <sup>19</sup>G. Calusine, A. Melville, W. Woods, R. Das, C. Stull, V. Bolkhovsky, D. Braje, D. Hover, D. K. Kim, X. Miloshi, D. Rosenberg, A. Sevi, J. L. Yoder, E. Dauler, and W. D. Oliver, "Analysis and mitigation of interface losses in trenched superconducting coplanar waveguide resonators," *Appl. Phys. Lett.* **112**, 062601 (2018).
- <sup>20</sup>A. P. Place, L. V. Rodgers, P. Mundada, B. M. Smitham, M. Fitzpatrick, Z. Leng, A. Premkumar, J. Bryon, A. Vrajitoarea, S. Sussman, G. Cheng, T. Madhavan, H. K. Babla, X. H. Le, Y. Gang, B. Jäck, A. Gynis, N. Yao, R. J. Cava, N. P. de Leon, and A. A. Houck, "New material platform for superconducting transmon qubits with coherence times exceeding 0.3 milliseconds," *Nat. Commun.* **12**, 1779 (2021).
- <sup>21</sup>J. T. Monroe, D. Kowsari, K. Zheng, C. Gaikwad, J. Brewster, D. S. Wisbey, and K. W. Murch, "Optical direct write of Dolan–Niemeyer–bridge junctions for transmon qubits," *Appl. Phys. Lett.* **119**, 062601 (2021).
- <sup>22</sup>J. Halbritter, "On the oxidation and on the superconductivity of niobium," *Appl. Phys. A* **43**, 1–28 (1987).
- <sup>23</sup>A. Nersisyan, E. A. Sete, S. Stanwyck, A. Bestwick, M. Reagor, S. Poletto, N. Alidoust, R. Manenti, R. Renzas, C.-V. Bui, K. Vu, T. Whyland, and Y. Mohan, "Manufacturing low dissipation superconducting quantum processors," in *IEEE International Electron Devices Meeting (IEDM)* (IEEE, 2019).
- <sup>24</sup>M. S. Blok, V. V. Ramasesh, T. Schuster, K. O'Brien, J. M. Kreikebaum, D. Dahmen, A. Morvan, B. Yoshida, N. Y. Yao, and I. Siddiqi, "Quantum information scrambling on a superconducting qutrit processor," *Phys. Rev. X* **11**, 021010 (2021).
- <sup>25</sup>D. Bach, H. Störmer, R. Schneider, D. Gerthsen, and J. Verbeek, "EELS investigations of different niobium oxide phases," *Microsc. Microanal.* **12**, 416–423 (2006).
- <sup>26</sup>D. Bach, "EELS investigations of stoichiometric niobium oxides and niobium-based capacitors," *Ph.D. thesis* (Universität Karlsruhe, 2009).
- <sup>27</sup>M. V. P. Altoé, A. Banerjee, C. Berk, A. Hajr, A. Schwartzberg, C. Song, M. A. Ghadeer, S. Aloni, M. J. Elowson, J. M. Kreikebaum, E. K. Wong, S. Griffin, S. Rao, A. Weber-Bargioni, A. M. Minor, D. I. Santiago, S. Cabrini, I. Siddiqi, and D. F. Ogletree, "Localization and reduction of superconducting quantum coherent circuit losses," *arXiv:2012.07604* (2020).
- <sup>28</sup>J. Verjauw, A. Potočnik, M. Mongillo, R. Acharya, F. Mohiyaddin, G. Simion, A. Pacco, T. Ivanov, D. Wan, A. Vanleenehove, L. Souriau, J. Jussot, A. Thiam, J. Swerts, X. Piao, S. Couet, M. Heyns, B. Govoreanu, and I. Radu, "Investigation of microwave loss induced by oxide regrowth in high-Q niobium resonators," *Phys. Rev. Appl.* **16**, 014018 (2021).
- <sup>29</sup>M. Siemers, A. Pflug, T. Melzig, K. Gehrke, A. Weimar, and B. Szyszka, "Model based investigation of Ar<sup>+</sup> ion damage in DC magnetron sputtering," *Surf. Coat. Technol.* **241**, 50–53 (2014).
- <sup>30</sup>F. M. D'Heurle, "Aluminum films deposited by rf sputtering," *Metall. Mater. Trans. B* **1**, 725–732 (1970).
- <sup>31</sup>S. Morohashi, N. Takeda, S. Tsujimura, M. Kawanishi, K. Harada, S. Maekawa, N. Nakayama, and T. Noguchi, "Characteristics of superconducting Nb layer

fabricated using high-vacuum electron beam evaporation," *Jpn. J. Appl. Phys., Part 1* **40**, 576–579 (2001).

<sup>32</sup>D. P. Pappas, M. R. Vissers, D. S. Wisbey, J. S. Kline, and J. Gao, "Two level system loss in superconducting microwave resonators," *IEEE Trans. Appl. Supercond.* **21**, 871 (2011).

<sup>33</sup>C. R. H. McRae, H. Wang, J. Gao, M. R. Vissers, T. Brecht, A. Dunsworth, D. P. Pappas, and J. Mutus, "Materials loss measurements using superconducting microwave resonators," *Rev. Sci. Instrum.* **91**, 091101 (2020).

<sup>34</sup>J. B. Chang, M. R. Vissers, A. D. Córcoles, M. Sandberg, J. Gao, D. W. Abraham, J. M. Chow, J. M. Gambetta, M. B. Rothwell, G. A. Keefe, M. Steffen, and D. P. Pappas, "Improved superconducting qubit coherence using titanium nitride," *Appl. Phys. Lett.* **103**, 012602 (2013).

<sup>35</sup>L. J. Zeng, P. Krantz, S. Nik, P. Delsing, and E. Olsson, "The atomic details of the interfacial interaction between the bottom electrode of Al/AlO<sub>x</sub>/Al Josephson junctions and HF-treated Si substrates," *J. Appl. Phys.* **117**, 163915 (2015).

<sup>36</sup>A. Premkumar, C. Weiland, S. Hwang, B. Jäck, A. P. M. Place, I. Waluyo, A. Hunt, V. Bisogni, J. Pelliciari, A. Barbour, M. S. Miller, P. Russo, F. Camino, K. Kisslinger, X. Tong, M. S. Hybertsen, A. A. Houck, and I. Jarrige, "Microscopic relaxation channels in materials for superconducting qubits," *Commun. Mater.* **2**, 72 (2021).

<sup>37</sup>B. Bonin and H. Safa, "Power dissipation at high fields in granular RF superconductivity," *Supercond. Sci. Technol.* **4**, 257–261 (1991).

<sup>38</sup>M. Newville, A. Ingargiola, T. Stensitzki, and D. B. Allen (2014). "LMFIT: Non-linear least-square minimization and curve-fitting for python," Zenodo. <https://doi.org/10.5281/zenodo.11813>.

<sup>39</sup>J. K. Hulm, C. K. Jones, R. A. Hein, and J. W. Gibson, "Superconductivity in the TiO and NbO systems," *J. Low Temp. Phys.* **7**, 291 (1972).

<sup>40</sup>M. R. Soares, S. Leite, C. Nico, M. Peres, A. J. Fernandes, M. P. Graça, M. Matos, R. Monteiro, T. Monteiro, and F. M. Costa, "Effect of processing method on physical properties of Nb<sub>2</sub>O<sub>5</sub>," *J. Eur. Ceram. Soc.* **31**, 501 (2011).

<sup>41</sup>C. Nico, T. Monteiro, and M. P. Graça, "Niobium oxides and niobates physical properties: Review and prospects," *Prog. Mater. Sci.* **80**, 1–37 (2016).

<sup>42</sup>J. Zmuidzinas, "Superconducting microresonators: Physics and applications," *Annu. Rev. Condens. Matter Phys.* **3**, 169–214 (2012).

<sup>43</sup>D. S. Wisbey, M. R. Vissers, J. Gao, J. S. Kline, M. O. Sandberg, M. P. Weides, M. M. Paquette, S. Karki, J. Brewster, D. Alameri, I. Kuljanishvili, A. N. Caruso, and D. P. Pappas, "Dielectric loss of boron-based dielectrics on niobium resonators," *J. Low Temp. Phys.* **195**, 474–486 (2019).

<sup>44</sup>J. Gao, "The physics of superconducting microwave resonators," *Ph.D. thesis* (California Institute of Technology, 2008).

<sup>45</sup>J. Burnett, L. Faoro, and T. Lindström, "Analysis of high quality superconducting resonators: Consequences for TLS properties in amorphous oxides," *Supercond. Sci. Technol.* **29**, 044008 (2016).

<sup>46</sup>A. Melville, G. Calusine, W. Woods, K. Serniak, E. Golden, B. M. Niedzielski, D. K. Kim, A. Sevi, J. L. Yoder, E. A. Dauler, and W. D. Oliver, "Comparison of dielectric loss in titanium nitride and aluminum superconducting resonators," *Appl. Phys. Lett.* **117**, 124004 (2020).